Received July 29, 2020, accepted September 2, 2020, date of publication September 7, 2020, date of current version September 22, 2020.

Digital Object Identifier 10.1109/ACCESS.2020.3022163

Synthesis of Dynamic Errors Correcting Algorithm for Auto–Balancing Bridge Methods

YURIY KHOMA[1], VOLODYMYR KHOMA[1,2], MICHAL PODPORA[2], (Member, IEEE), ALEKSANDRA KAWALA-STERNIUK[2], (Member, IEEE), RADEK MARTINEK[3], (Member, IEEE), AND STEPAN OZANA[3]

[1]Department of Information Measurement Technologies, Lviv Polytechnic National University, 79013 Lviv, Ukraine
[2]Faculty of Electrical Engineering, Automatic Control and Informatics, Opole University of Technology, 45-758 Opole, Poland
[3]Department of Cybernetics and Biomedical Engineering, VSB-Technical University Ostrava – FEECS, 708 00 Ostrava–Poruba, Czechia

Corresponding authors: Volodymyr Khoma (v.khoma@po.edu.pl) and Michal Podpora (m.podpora@po.edu.pl)

This work was supported in part by the European Regional Development Fund in the Research Centre of Advanced Mechatronic Systems project, project number *CZ*.02.1.01/0.0/0.0/16_019/0000867 within the Operational Programme Research, Development and Education and by the project *SP*2020/42, ''Development of algorithms and systems for control, measurement and safety applications VI'' of Student Grant System, VSB-TU Ostrava.''

ABSTRACT Autobalancing bridge method is widely used to measure the impedance of various objects in many fields of science and technology. The article presents an innovative approach to address auto-balancing bridge dynamic errors to extend the range of operating frequencies. The mathematical model of auto-balancing bridge, implemented using operational amplifier, was analysed, obtaining its simplified version taking into account the most important sources of errors. The concept was developed and the algorithms for compensation of the impact of dynamic errors on the measurement of admittance components were synthesized. The presented algorithms allow the correction of admittance measurements only based on ''raw'' results obtained with the use of an auto-balancing bridge. Methodology was described and numerical simulation was carried out on a selected example. As shown in the paper, the developed correction algorithms allow extending significantly (400 times) the range of admittance measurement frequencies. These algorithms do not require interfering the auto-balancing bridge structure, but only engage the computing power of modern measurement channels.

INDEX TERMS Auto-balancing bridge method, conductance and susceptance measurement, correction algorithms, dynamic errors in frequency domain, mathematical model of operational circuit, multi–frequency impedance meter.

I. INTRODUCTION

Measurement of impedance, as the object's response to an alternating current flow, is increasingly used not only in the study of electronic components, but also in many other fields, for example in chemistry, medicine, materials science [1]–[8]. By measuring impedance, it is possible to test numerous physical quantities and technological parameters.

Measurement of complex impedance of various biological tissues is called bioimpedance spectroscopy. It is a very promising tool for the purpose of diagnostic measurements such as: body composition, blood pressure, blood characteristic etc… [9]. Implementation of impedance is very popular in various healthcare applications, where bio-impedance is frequently combined with analysis of other signals, such as electrocardiography (ECG) or electro-dermal activity data [10]–[12].

Automatic balancing bridges require simple and efficient strategies, which may be implemented on various controllers. For the problem resolving or errors reduction require various sophisticated methods such as inter alia Broyden's method [13]. Thus, the problem is strongly related with the higher frequencies, which is not the scope of this work, further investigation of this topic was not carried out of the authors of this work.

One of the main disadvantages of using auto-balancing bridge method is the number of measuring points. They are very popular in numerous lab environments. The basic

The associate editor coordinating the review of this manuscript and approving it for publication was Jenny Mahoney.

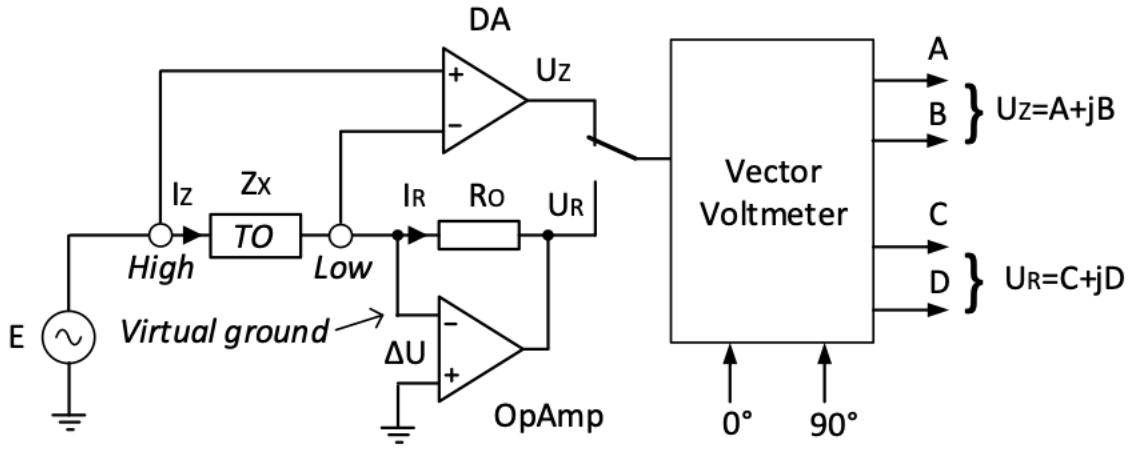

FIGURE 1. Principle of the auto-balancing bridge method.

functionality and Schematic of such bridges was presented in detail in the following literature: [14]–[17].

There are several methods of measuring impedance, each of which has its advantages and disadvantages, and the choice of the appropriate one depends primarily on the ranges of measured impedance parameters, the required accuracy and speed of measurement, the range of the test signal frequency and simplicity of operation. The most accurate and very popular in laboratory environments is the bridge method, however, it still has some significant limitations related with the complexity of the balancing process realisation. It results with the extension of the measurement time and increases the hardware expenditure [13]–[15], [18]. The so-called auto-balancing bridge method is simple to implement and combines numerous advantages, primarily high measurement speed [18], [19].

Impedance measurement methods can be divided into two categories. The first one is related with the ''single-tones'' data, which means that only pure frequency sine is applied for the purpose of measurement. The analysis of the first type is quite simple and does not require sophisticated signal processing methods. The second one is correlated with the ''multi-tone'' signals and it allows to analyse the whole frequency range at the same time, however it requires implementation of more advances signal processing methods. Both methods require high computing power and are very time consuming [9].

The essence of auto-balancing bridge method is explained in Figure 1. As a result of excitation with sinusoidal voltage E of the tested object TO with impedance Z_X, current I_Z flows through it. This current is balanced by the I_R current produced by the I/U converter built in a conventional manner on an operational amplifier ($OpAmp$) with a range resistor R_O in a feedback loop. Assuming ideal $OpAmp$ parameters, the ΔU potential on the Low terminal (called virtual ground) is zero, therefore the voltage drop across the impedance measured U_Z is the same as the excitation signal E. So the measured impedance can be calculated from the following formula (1):

$$\mathrm{Z_X} = -\mathrm{R_O}\frac{\mathrm{U_Z}}{\mathrm{U_R}}. \tag{1}$$

To measure U_Z and U_R voltages as complex values, a vector voltmeter is used, which is driven with 0° and 90° reference phase signals to extract the real and imaginary components (A and $j \cdot B$) of the U_Z signal and the components (C and $j \cdot D$) of the U_R signal. Thus the resistance R and the reactance X of measurand Z_X is represented by the following equations ((2)):

$$\mathrm{R} = \mathrm{R_O}\frac{\mathrm{A}\cdot\mathrm{C}+\mathrm{B}\cdot\mathrm{D}}{\mathrm{C}^2+\mathrm{D}^2}; \quad \mathrm{X} = \mathrm{R_O}\frac{\mathrm{B}\cdot\mathrm{C}-\mathrm{A}\cdot\mathrm{D}}{\mathrm{C}^2+\mathrm{D}^2}. \tag{2}$$

The development of integrated circuit technology, including digital signal processing techniques, now allows high-precision synthesis and measurement of orthogonal voltage components in a wide frequency range. For example, in the Analog Devices AD5933 and AD5934 transducers, a discrete Fourier Transform algorithm is used for measurement of impedance components [7], [20]–[23]. There are also alternative approaches to voltage conversion U_Z and U_R. For example, in paper [24] algorithm combining oversampling and digital lock-in amplifier, in [25] – information-filtering demodulation method, in [26] – approach based on multi-frequency excitation and Fourier analysis in frequency domain. The main source of the measurement errors in this case is auto-balancing bridge section.

The previous literature study shows (see: [18], [23], [27]) that the auto-balancing bridge errors are inherently dynamic errors because they are a result of energy accumulation primarily in the parasitic capacities of the operational amplifier, which inter alia causes virtual ground potential to be $\Delta U \neq 0$. So the voltage U_Z should be separated with using differential amplifier (DA) as a potential difference on High and Low terminals of the tested object. However, this solution can be used at frequencies below 100 kHz [18].

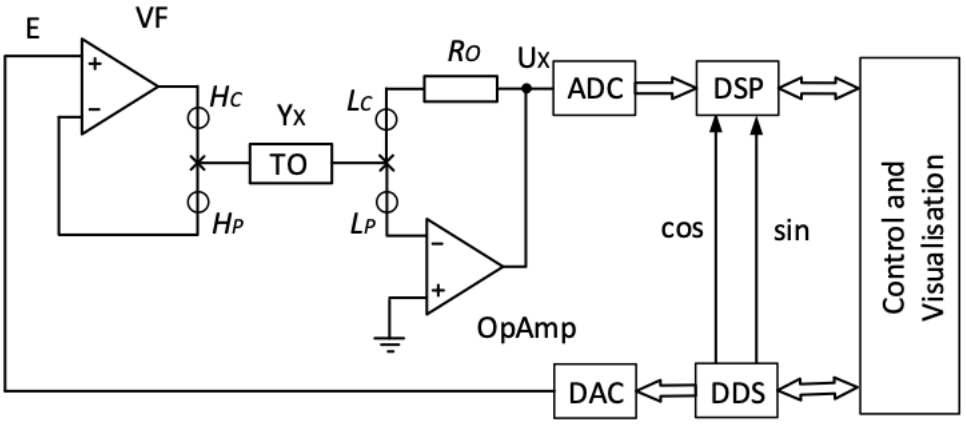

FIGURE 2. Block diagram of a multi–frequency impedance meter based on auto-balancing bridge method.

Improvement of the impedance measurement accuracy in the frequency range over 100 kHz is obtained by structural changes of the I/U converter. For example, Keysight Technologies (formerly Agilant) is expanding the I/U converter with a zero detector (a null detector), phase sensitive detectors, integrator and vector modulators, ensuring high level of gain for high frequencies (up to 120 MHz) [18].

Thus, in known impedance meters, there is a need to measure the ratio of two complex voltages U_R and U_Z according to equations (2). This results in time redundancy and provides impedance measurements only up to 100 kHz. Extending the frequency range over 100 kHz is possible by additional hardware upgrade of the I/U converter, i.e. it is achieved at the expense of increasing the equipment complexity.

Most of the modern bioelectrical impedance spectroscopy systems are partially based on the above mentioned auto–balancing bridge methods [28], [29]. Therefore this paper presents an alternative way of extending the impedance meter frequency range, which does not require changing the auto–balancing bridge structure. The essence of the proposed method is software-based dynamic error correction, which only requires the involvement of appropriate computing power that modern measurement equipment has. The implementation of the proposed approach requires above all the synthesis of relevant correction algorithms.

The aim of the paper is to present a new idea of increasing the frequency range of auto-balancing bridge section, which is the basic part of the multi-frequency impedance meter. The innovation of the proposed solution is based on the use of computational power in order to correct dynamic errors, and not to introduce the structural redundancy, as it is used in already known solutions. In order to implement such a solution in practice it is necessary to synthesize appropriate algorithms, which is the essence of the matter.

The scope of the article includes the description of the structure of multi-frequency meter based on the auto-balancing bridge method, analysis and formalization of the mathematical model of auto-balancing bridge circuit, constituting the basis for the synthesis of correction algorithms. The scope of the article also includes a description of the methodology for testing the effectiveness of the above algorithms. The results of the numerical simulation carried out using PSpice model showed that the proposed solution extends the frequency range of admittance measurement 400 times, by omitting other sources of error.

II. MATERIALS AND METHODS

The authors of this work focused on implementation and also on potential of the auto–balancing bridge method, which is one of the methods with the widest potential application used for the impedance measurement purposes [30].

A. BLOCK DIAGRAM AND OPERATION PRINCIPLE OF THE MULTI–FREQUENCY IMPEDANCE METER BASED ON AUTO–BALANCING BRIDGE METHOD

The proposed method of dynamic error correction can be used in order to build a multi–frequency impedance meter, a block diagram of which is shown in Figure 2.

The analog section of the system implementing the auto–balancing bridge method is built with an I/U converter based on *OpAmp*, range resistor R_O and voltage follower (VF). The tested object is connected to the impedance meter using two current cables (H_C and L_C) and two potential cables (H_P and L_P). Using voltage follower on the High terminals side ensures invariability of the impact of the parasitic parameters of these wires on the accuracy of impedance measurement. Impact of the Low current terminal (L_C) can be eliminated during calibration of the measuring path. Whereas the Low potential terminal (L_P) cable impedance is added to the high input impedance of *OpAmp*, therefore its influence is mitigated.

The U_X voltage at the output of the analog section in the first approximation (in terms of possible dynamic errors) is proportional not to the impedance Z_X of the tested object,

but to its reciprocal – called admittance Y_X (3):

$$\mathrm{U_X} \approx -\mathrm{Y_X} \cdot \mathrm{R_O} \cdot \mathrm{E} = \left[\mathrm{G_X} \cdot \mathrm{R_O} + \mathrm{jB_X} \cdot \mathrm{R_O}\right] \times \mathrm{E} \quad (3)$$

where: G_X is the active component of admittance (conductance), and B_X is the reactive component (susceptance).

So the values of conductance and susceptance are obtained as the results of the in-phase and quadrature measurements of the U_X voltage component relative to test signal E. For this purpose, the instantaneous voltage values were converted to digital form $U_{X(n)}$ using ADC (Analog to Digital Converter). The DSP (Digital Signal Processing) unit, based on orthogonal reference digital signals *sin* and *cos*, reduces the complex voltage U_X to the real and imaginary part according to the One-Point Discrete Fourier Transform algorithm [21]–[23] (4) and (5):

$$\mathrm{M_1} = \mathrm{real}\left(\mathrm{U_X}\right) = \sum_{\mathrm{n=0}}^{\mathrm{N-1}} \mathrm{U_X(n)} \cdot \cos\left(2\pi\,\mathrm{fnT_S}\right), \quad (4)$$

$$\mathrm{M_2} = \mathrm{imag}\left(\mathrm{U_X}\right) = \sum_{\mathrm{n=0}}^{\mathrm{N-1}} \mathrm{U_X(n)} \cdot \sin\left(2\pi\,\mathrm{fnT_S}\right) \quad (5)$$

where:

- T_S – sampling period;
- n – sample number in the block;
- N – total number of samples in the block;
- $cos(n)$ and $sin(n)$ are the sampled test vectors provided by the DDS core at the frequency point f.

If the in-phase condition of the excitation signal E and the reference signal $cos(n)$ is ensured, the obtained according to (4) and (5) quantities M_1 and M_2 will reflect conductance and susceptance of the tested object (6):

$$\mathrm{M_G} = \mathrm{M_1} \quad \text{and} \quad \mathrm{M_B} = \mathrm{M_2}. \quad (6)$$

Test signal E and reference signals *sin* and *cos* are generated using the Digital Direct Synthesis (DDS) technique, which ensures high resolution frequency tuning while maintaining high stability [23], [31], [32]. The DAC (Digital to Analog Converter) is used to form the excitation voltage E. A common reference voltage source for DAC and ADC (Fig. 2) will ensure that there is no dependence of measurements up to its value.

In the single-channel meter structure, the generator and vector voltmeter can be a source of amplitude and phase errors, especially at higher frequencies. The systematic component of these errors can be compensated at the calibration stage of the measurement path. For this purpose, instead of U_X, excitation signal E is fed to the ADC input (Fig. 2) and its real (C) and imaginary (D) parts are measured at all frequency points. Thus, the error compensation of the generator and vector voltmeter is possible in the manner of calculations according to formula (2).

The limited dynamics of operational amplifier causes dynamic I/U converter errors to appear and increase in value as the frequency of the excitation signal increases. As a result, the M_G and M_B values calculated in the DSP unit are affected by errors and only in the first approximation they represent conductance and susceptance of tested object. In order to reduce these errors, the "raw" results of M_G and M_B measurements are processed by a computer (PC) using special algorithms, which allows the extension of the frequency range of multi–frequency impedance meter.

Based on the G and B admittance components, it is more convenient to describe the properties of objects using a parallel equivalent circuit, and if necessary, by means of conventional calculations using PC, impedance parameters (resistance R and reactance X) can be obtained for the serial equivalent circuit [18]. In addition, a PC can be also used for calculating other impedance parameters, e.g. quality factor Q, dissipation factor D, magnitude $|Z|$ phase angle θ, etc. [18], [27].

The peculiarity of the proposed multi–frequency impedance meter solution compared to known systems is the single–channel measurement path, which is convenient for the construction of simple portable devices.

B. ANALYSIS AND FORMALIZATION OF THE MATHEMATICAL MODEL OF THE AUTO-BALANCING BRIDGE

The mathematical model of any operational circuit with a single operational amplifier, which fully takes into account its properties in frequency domain, can be reduced to the canonical form of the transfer function [33] (7):

$$\mathrm{H} = \left(\mathrm{H_\infty} + \frac{\mathrm{H_0}}{\mathrm{A} \cdot \beta}\right) \cdot \frac{1}{1 + (\mathrm{A} \cdot \beta)^{-1}} \quad (7)$$

where:

- A – open-loop gain of *OpAmp*;
- β – feedback factor of operational circuit;
- H_∞ — idealized closed–loop gain at $A = \infty$;
- H_0 – feed–forward gain at $A = 0$.

In the particular case of the operating circuit built according to the auto-balancing bridge method (Figure 3), the above-mentioned elements of equation (7) can be specified. The idealized closed-loop gain is defined as the impedance ratio of $Z_2 = R_O$ in the *OpAmp* feedback loop and at its input $Z_1 = Z_X$:

$$\mathrm{H_\infty} = -\frac{\mathrm{Z_2}}{\mathrm{Z_1}} = -\frac{\mathrm{R_O}}{\mathrm{Z_X}} = -\mathrm{R_O Y_X}. \quad (8)$$

In the equation above, impedance is given in the form of its inverse – as admittance $Y_X = 1/Z_X$, which allows replacement of the division by the product.

In turn, the $H_0/(A \cdot \beta)$ term in expression (7) basically takes into account the direct signal propagation, which results from the non-zero value of the output impedance R_{OUT} of *OpAmp*, and for the considered auto-balancing bridge system it is described by the following formula (9):

$$\frac{\mathrm{H_0}}{\mathrm{A} \cdot \beta} = \frac{\mathrm{R_{OUT}}}{\mathrm{A} \cdot \mathrm{Z_1}} = \frac{\mathrm{R_{OUT}} \cdot \mathrm{Y_X}}{\mathrm{A}}. \quad (9)$$

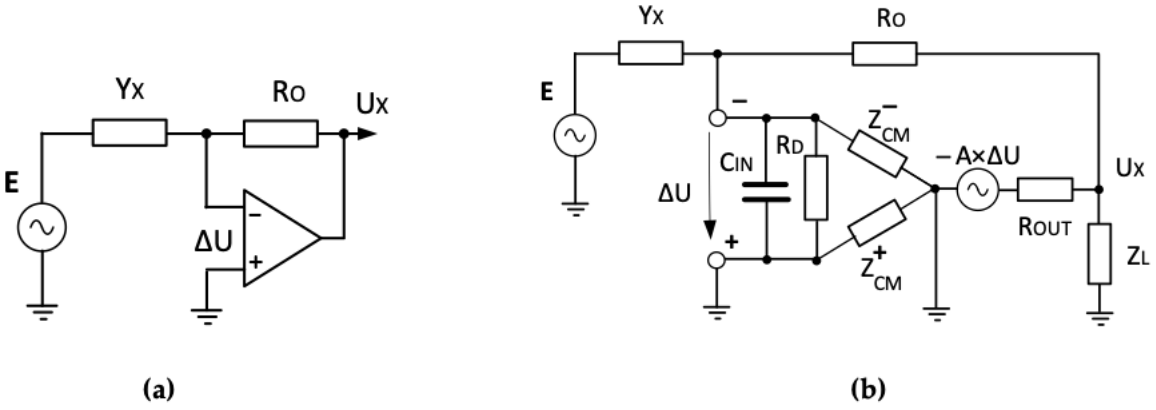

FIGURE 3. Auto–balancing bridge circuit (a) and equivalent circuit (b) for calculation components of its closed–loop gain *H*.

The majority of the operational amplifiers have a gain frequency response, which can be accurately approximated by a simple one–pole response [33], [34] (10):

$$\mathrm{A} = \frac{\mathrm{A}_0}{1 + \mathrm{j}\frac{\mathrm{f}}{\mathrm{f_T}}\mathrm{A}_0} \tag{10}$$

where:

- A_0 – DC open–loop gain;
- f_T – unity gain frequency;
- f – test signal frequency;
- j – designation of the imaginary part.

According to definition, the feedback factor β is the ratio of the *OpAmp* internal input voltage ΔU to its internal output voltage E_{OUT}. Basically, the feedback factor β represents the transmittance of the passive divider, at the input of which there is E_{OUT} voltage, and at the output: ΔU. The β factor takes into account most of the actual *OpAmp* parameters and has a decisive impact on the behaviour of operational circuit in a frequency domain. Because in the formulas (7) and (9) the coefficient β occurs only in the denominator, it is easier to use its inverse, i.e. $1/\beta$ (11):

$$\frac{1}{\beta} = \left(1 + \frac{\mathrm{Z_2}}{\mathrm{Z_1}} + \frac{\mathrm{Z_2}}{\mathrm{Z_P}}\right)\left(1 + \frac{\mathrm{R_{OUT}}}{\mathrm{Z_L}}\right) + \frac{\mathrm{R_{OUT}}}{\mathrm{Z_1}} + \frac{\mathrm{R_{OUT}}}{\mathrm{Z_P}} \tag{11}$$

where:

- Z_L – a load impedance;
- $Z_P = 1/Y_P = Z_D \,||\, Z_{S^-}$ – an input equivalent impedance (admittance);
- Z_D – the *OpAmp* differential input impedance;
- Z_{S^-} – the *OpAmp* common mode input impedance.

By substituting using the expressions (8), (9) and (11) the result enables calculation (8), an actual transfer function of the auto–balancing bridge is obtained, which includes *OpAmp* and feedback loop parameters and reflects sources of frequency errors (12), as shown at the bottom of the next page.

The equation (12) is quite complex, which may make its potential application in engineering practice difficult. Therefore some simplifications, which will not significantly affect the adequacy of the model, were introduced. First of all, the R_{OUT}/Z_L component can be omitted, because the default values of the output resistance of operational amplifiers range up to several tens of ohms, and load impedance can reach hundreds of kilo-Ohms and more, i.e. $R_{OUT}/Z_L \ll 1$. In expression (9) the inverse $1/A_0$ can also be omitted due to the fact that at the frequencies where the dynamic errors are already noticeable, its value will be insignificant compared to the f/f_T ratio.

It should also be noted that in the aforementioned frequency range, the C_{IN} operational amplifier input capacity will contain difference resistance R_D and input common mode resistance R_{S^-}, so the Z_P can be written as (13):

$$\mathrm{Z_P} = \frac{\mathrm{R_D R_{S-}}}{2 + \mathrm{j}\omega\mathrm{C_{IN} R_D R_{S-}}} \approx \frac{1}{\mathrm{j}\omega\mathrm{C_{IN}}}. \tag{13}$$

Also, if the product $Y_X \cdot R_0$ is excluded from the numerator of the expression (11), then the actual transfer function of the auto-balancing bridge takes the following form (14), as shown at the bottom of the next page.

An examination of the adequacy of the obtained simplified model of the auto—balancing bridge (14) showed that the divergence of the full model (12) does not exceed 0.01%. The confirmation of the adequacy of the obtained simplified model of the auto-balancing bridge (14) are the results of the simulations presented in Tables 1 and 2. In addition, comparative analysis of transmittance equations of a circuit based on an ideal operational amplifier (8) and the one built on *OpAmp* with real parameters (14) has allowed to determine that the most significant sources of errors are: decrease in gain A with frequency increase, influence of output impedance R_{OUT} of the operational amplifier and the impact of its C_{IN} input capacity.

In order to make it easier to see the nature of the relationship between different operating circuit parameters in numerator and denominator polynomials, the model (14) should be formalized by introducing symbolic variables, described below.

TABLE 1. Dynamic error of conductance measurement of tested object of admittance $Y_X = 10 + j100\,[\mu S]$.

f, Hz	10	10^2	10^3	10^4	$\sim \mathbf{1.2 \times 10^4}$	10^5	10^6	$\sim \mathbf{5.9 \times 10^6}$
$\delta_{G'}\%$	0.01	0.016	0.08	0.8	**1.0**	7.6	88	**>100**
$\varepsilon_{G'}\%$	0.01	0.01	0.01	0.01	**0.01**	0.017	0.09	**1.0**

TABLE 2. Dynamic errors of susceptance measurement of tested object of admittance $Y_X = 100 + j10\,[\mu S]$.

f, Hz	10	10^2	10^3	$\sim \mathbf{7.9 \times 10^3}$	10^4	10^5	10^6	$\sim \mathbf{4 \times 10^6}$
$\delta_{B'}\%$	-0.01	-0.016	-0.13	**-1.0**	-1.2	-12.5	>-100	**>-100**
$\varepsilon_{B'}\%$	-0.01	-0.01	-0.01	**-0.01**	-0.01	-0.013	-0.1	**-1.0** %

The $Y_X \cdot R_O$ product can be interpreted as normalized impedance measurement results, therefore they were named (15):

$$\mathrm{Y_X \cdot R_O = G + j \cdot B} \tag{15}$$

where G and B – respectively: normalized active (conductance) and reactive (susceptance) components of the admittance of the measured object.

The ratio of the output resistance R_{OUT} to the resistance of the reference resistor R_O is denoted with the frequency independent variable D, while the product of the input capacity C_{IN} in formalized model is represented by the variable C, proportionally dependent on the frequency (16) and (17):

$$\mathrm{D} = \frac{\mathrm{R_{OUT}}}{\mathrm{R_O}}, \tag{16}$$

$$\mathrm{C} = \omega \mathrm{C_{IN} R_O}. \tag{17}$$

And the ratio of the frequency of a single gain to the frequency of the sampling signal is denoted as (18):

$$\mathrm{K} = \frac{\mathrm{f_T}}{\mathrm{f}}. \tag{18}$$

Thus, the formalized mathematical model of the auto-balancing bridge taking into account variables from (15) – (18) is expressed with (19), as shown at the bottom of the next page.

The products $Y_X \cdot R_{OUT}$ and $\omega \cdot C_{IN} \cdot R_{OUT}$ can also be expressed by the variables D and C as follows (20) and (21):

$$\mathrm{Y_X R_{OUT}} = \mathrm{Y_X R_O} \frac{\mathrm{R_{OUT}}}{\mathrm{R_O}} = \mathrm{D(G + jB)}, \tag{20}$$

$$\omega \mathrm{C_{IN} R_{OUT}} = \omega \mathrm{C_N R_O} \frac{\mathrm{R_{OUT}}}{\mathrm{R_O}} = \mathrm{C \cdot D}. \tag{21}$$

The finally formalized mathematical model of the auto–balancing bridge is as follows (22):

$$\mathrm{H} = \frac{(\mathrm{G + jB})\left(1 - \mathrm{j}\frac{\mathrm{D}}{\mathrm{K}}\right)}{1 + \mathrm{j}\frac{1}{\mathrm{K}}[1 + (\mathrm{G + jB})(1 + \mathrm{D}) + \mathrm{jC}(1 + \mathrm{D})]}. \tag{22}$$

Each of the variables K, C and D discussed above in the model (22) reflects one of the three main sources of dynamic error occurring in the auto-balancing bridge:

- variable K – decrease in the amplification factor A of the operational amplifier relative to the increase in frequency f;
- variable C – short circuit with input capacitance C_{IN} of input differential resistance and common mode ratio resistance;
- variable D – direct signal transmissions from input to output of the operating circuit due to non-zero operational amplifier output resistance.

C. CORRECTION ALGORITHM's SYNTHESIS CONCEPT

The starting point for the synthesis of the correction algorithm will be the formalized model (22) obtained in the previous subsection. Let's extract the real part P and the imaginary part Q (23), as shown at the bottom of the next page.

This means that P and Q values can be interpreted as "approximate" impedance measurement results, because the "ideal" results according to (8) and (15) are (24):

$$\mathrm{H_\infty = -Y_X \cdot R_O = G + j \cdot B}. \tag{24}$$

The synthesis of correction algorithms involves the following steps. First, let's get rid of the denominator in expression (23) by multiplying the right and left sides by the denominator, resulting (25), as shown at the bottom of the next page.

$$\mathrm{H} = -\frac{\mathrm{Y_X R_O} - \frac{\mathrm{Y_X R_{OUT}}}{\mathrm{A}}}{1 + \frac{1}{\mathrm{A}}\left[(1 + \mathrm{Y_X R_O} + \mathrm{Y_P R_O})\left(1 + \frac{\mathrm{R_{OUT}}}{\mathrm{Z_L}}\right) + \mathrm{Y_X R_{OUT}} + \mathrm{Y_P R_{OUT}}\right]} = \mathrm{real(H)} + j \cdot \mathrm{imag(H)}. \tag{12}$$

$$\mathrm{H} = \frac{-\mathrm{Y_X R_o}\left(1 - \mathrm{j}\frac{\mathrm{f}}{\mathrm{f_T}} \cdot \frac{\mathrm{R_{OUT}}}{\mathrm{R_O}}\right)}{1 + \mathrm{j}\frac{\mathrm{f}}{\mathrm{f_T}}\left[1 + \mathrm{Y_X R_O} + \mathrm{j}\omega \mathrm{C_{IN} R_O} + \mathrm{Y_X R_{OUT}} + \mathrm{j}\omega \mathrm{C_{IN} R_{OUT}}\right]}. \tag{14}$$

By writing separately the real and imaginary parts in the above statement (25), the system of two equations in real numbers is obtained (26), as shown at the bottom of the next page.

After regrouping words relative to G and B, and after moving the independent variables to the left, the equation is transferred into (27), as shown at the bottom of the next page.

By introducing the following notations (28) – (31):

$$\mathrm{a} = 1 + \mathrm{Q}\frac{(1+\mathrm{D})}{\mathrm{K}}, \tag{28}$$

$$\mathrm{b} = \mathrm{P}\frac{(1+\mathrm{D})}{\mathrm{K}}, \tag{29}$$

$$\mathrm{c} = \mathrm{P} - \mathrm{P}\cdot\mathrm{C}\frac{(1+\mathrm{D})}{\mathrm{K}} - \frac{\mathrm{Q}}{\mathrm{K}}, \tag{30}$$

$$\mathrm{d} = \mathrm{Q} - \mathrm{Q}\cdot\mathrm{C}\frac{(1+\mathrm{D})}{\mathrm{K}} + \frac{\mathrm{P}}{\mathrm{K}} \tag{31}$$

the solution of this system of equations can be written in the following form (32) and (33):

$$\mathrm{G} = \frac{\mathrm{a}\cdot\mathrm{c} - \mathrm{b}\cdot\mathrm{d}}{\mathrm{a}^2 + \mathrm{b}^2}, \tag{32}$$

$$\mathrm{B} = \frac{\mathrm{b}\cdot\mathrm{c} + \mathrm{a}\cdot\mathrm{d}}{\mathrm{a}^2 + \mathrm{b}^2}. \tag{33}$$

In fact, there are no quantities P and Q, because they represent real and imaginary components of simplified model 14. The "raw" measurement results are the corresponding *real*$\{H\}$ and *imag*$\{H\}$ transfer function components of the full model (12), which in practice can be obtained by using U_X One–Point Fourier Transform for the output voltage, as in equations 4 and 5 resulting with the below formulae 34:

$$\mathrm{real}\{\mathrm{H}_\infty\} = \mathrm{M_G} \quad \text{and} \quad \mathrm{imag}\{\mathrm{H}_\infty\} = \mathrm{M_B}. \tag{34}$$

Therefore, if in formulas (28) – (31) the following (35) will be replaced:

$$\mathrm{P} \to \mathrm{M_G} = \mathrm{real}\{\mathrm{H}_\infty\} \quad \text{and} \quad \mathrm{Q} \to \mathrm{M_B} = \mathrm{imag}\{\mathrm{H}_\infty\} \tag{35}$$

the algorithm formulas (36) and (37) for correction will be obtained:

$$\widetilde{\mathrm{G}} = \frac{\widetilde{\mathrm{a}}\cdot\widetilde{\mathrm{c}} - \widetilde{\mathrm{b}}\cdot\widetilde{\mathrm{d}}}{\widetilde{\mathrm{a}}^2 + \widetilde{\mathrm{b}}^2} = \mathrm{N_G}, \tag{36}$$

$$\widetilde{\mathrm{B}} = \frac{\widetilde{\mathrm{b}}\cdot\widetilde{\mathrm{c}} + \widetilde{\mathrm{a}}\cdot\widetilde{\mathrm{d}}}{\widetilde{\mathrm{a}}^2 + \widetilde{\mathrm{b}}^2} \tag{37}$$

where (38) – (41):

$$\widetilde{\mathrm{a}} = 1 + \mathrm{M_B}\frac{(1+\mathrm{D})}{\mathrm{K}}, \tag{38}$$

$$\widetilde{\mathrm{b}} = \mathrm{M_G}\frac{(1+\mathrm{D})}{\mathrm{K}}, \tag{39}$$

$$\widetilde{\mathrm{c}} = \mathrm{M_G} - \mathrm{M_G}\cdot\mathrm{C}\frac{(1+\mathrm{D})}{\mathrm{K}} - \frac{\mathrm{M_B}}{\mathrm{K}}, \tag{40}$$

$$\widetilde{\mathrm{d}} = \mathrm{M_B} - \mathrm{M_B}\cdot\mathrm{C}\frac{(1+\mathrm{D})}{\mathrm{K}} + \frac{\mathrm{M_G}}{\mathrm{K}}. \tag{41}$$

The algorithm's input includes both M_G M_B measurement results with dynamic errors, and its output gives more accurate N_G and N_B results close to the true values of conductance G_X and susceptance B_X of measurand Y_X.

D. NUMERICAL SIMULATION's METHODOLOGY

The main purpose of the proposed algorithm (38) – (41) is the correction of dynamic errors arising at the stage of processing Y_X admittance to the proportional complex voltage U_X. Therefore, it is important to explore the possibility of extending the frequency range using correction algorithms in multi–frequency impedance meter.

For the study purposes the AD845 precision operational amplifier (Analog Devices) with the following parameters was used in order to verify the correction algorithms [35]:

- $A_0 = 100000$;
- $f_T = 16\,MHz$;
- $R_D = 10\,M\Omega$;
- $C_{IN} = 4\,pF$;
- $R_{OUT} = 5\Omega$;
- $R_{S^-} = 100\,M\Omega$;
- $R_L = 10\,k\Omega$

.

Initially, based on the model (12), observations were made of dynamic errors of the auto–balancing bridge occurring on the phase plane $G = G_X \cdot R_O = 0 \div 1.0$ and $B = B_X \cdot R_O = 0 \div 1.0$. The two quantities D and C, according to (16) and (17) negatively affecting the measurement accuracy, maintain a controversial relationship with the reference resistance R_O,

$$\mathrm{H} = -\frac{(\mathrm{G}+\mathrm{jB})(1-\mathrm{j}\frac{\mathrm{D}}{\mathrm{K}})}{1+\mathrm{j}\frac{1}{\mathrm{K}}\left[1+(\mathrm{G}+\mathrm{jB})+\mathrm{jC}+\mathrm{Y_x}\mathrm{R_{OUT}}+\mathrm{j}\omega\mathrm{C_{IN}}\mathrm{R_{OUT}}\right]}. \tag{19}$$

$$\mathrm{H} = \mathrm{P}+\mathrm{j}\cdot\mathrm{Q} = -\frac{(\mathrm{G}+\mathrm{jB})\left(1-\mathrm{j}\frac{\mathrm{D}}{\mathrm{K}}\right)}{1+\mathrm{j}\frac{1}{\mathrm{K}}[1+(\mathrm{G}+\mathrm{jB})(1+\mathrm{D})+\mathrm{jC}(1+\mathrm{D})]}. \tag{23}$$

$$\mathrm{P}+\mathrm{jQ}+\mathrm{j}\frac{(\mathrm{P}+\mathrm{jQ})}{\mathrm{K}}[1+(\mathrm{G}+\mathrm{jB})(1+\mathrm{D})+\mathrm{jC}(1+\mathrm{D})] = (\mathrm{G}+\mathrm{jB})\left(1-\mathrm{j}\frac{\mathrm{D}}{\mathrm{K}}\right). \tag{25}$$

the proportional C, and the inverse D. In: [18] criteria were introduced to roughly discriminate between low, middle, and high impedance. The reference resistance $R_O = 10\ k\Omega$ corresponds to the middle sub–range of the measurement [18], therefore the research concerned conductance and susceptance measurements from 0 to $10^{-4}S$.

The calibration of the measuring path is aimed at the correcting additive and multiplicative errors. Elimination of the additive error consists in carrying out measurements in the open compensation mode, i.e. when $G = 0$ and $B = 0$. To eliminate the multiplicative error, measurements are performed in the load compensation mode using the reference resistor $R_C = R_O$, i.e. $G = 1$ and $B = 0$.

The calibration of the measuring path is aimed at the correcting additive and multiplicative errors. Admittance measurements are accompanied by additive and multiplicative errors. The main source of additive errors are the residuals of a test cables. In the open compensation mode the DUT contact terminals are opened, i.e. when $G = 0$ and $B = 0$. So the measurement result reflects the stray conductance G_S and susceptance B_S. To eliminate these residuals, the G_S and B_S values should be subtracted from the measured admittance components. To minimize the multiplicative error, measurements are performed in the load compensation mode using the reference resistor $R_C = R_O$, i.e. $G = 1$ and $B = 0$.

Figure 4 presents the results of numerical simulation of the accuracy of measurement with an auto–balancing bridge at the frequency $f = 1\ MHz$ of admittance components (in relative form M_G/G and M_B/B).

From the obtained results it can be concluded that the least favourable measurement conditions occur when the measured admittance component is small in relation to the second component (when dynamic errors reach up to 15%). Therefore, adverse conditions were selected for further analysis when the controlled impedance component is only about 10% of its module, which corresponded to:

- measurement of the active component $G = G_X \cdot R_O = 10\,[\mu S] \cdot 10\,[k\Omega] = 0.1$ in favour of the reactive component $B = B_X \cdot R_O = 100\,[\mu S] \cdot 10\,[k\Omega] = 1.0$;
- measurement of the reactive component, smaller in value, $B = B_X \cdot R_O = 10\,[\mu S] \cdot 10\,[k\Omega] = 0.1$ with the dominant active component $G = G_X \cdot R_O = 100\,[\mu S] \cdot 10\,[k\Omega] = 1.0$

III. RESULTS

To estimate dynamic errors of the auto-balancing bridge, formulas are used to calculate the relative error of conductance and susceptance before correction (42) and (43):

$$\delta_G = (\frac{M_G}{G} - 1) \times 100\%, \tag{42}$$

$$\delta_B = (\frac{M_B}{B} - 1) \times 100\%, \tag{43}$$

and after applying correction algorithms (44) and (45):

$$\varepsilon_G = (\frac{N_G}{G} - 1) \times 100\%, \tag{44}$$

$$\varepsilon_B = (\frac{N_B}{B} - 1) \times 100\%. \tag{45}$$

The M_G and M_B quantities were calculated from formulas (12) and (34), while N_G and N_B from formulas (38) – (41).

Since the dynamic error in the measurement of admittance components depends on the ratio of their value, the worst case was chosen for conductance measurement against the background of 10 times higher susceptance (Table 1) and similarly, the measurement of susceptance against the background of 10 times higher conductance (Table 2). The results of the numerical simulation were made based on the parameters of the PSpice model of the AD845 operational amplifier in the frequency range from 10 Hz to several MHz, on which dynamic error after applying correction algorithms reaches 1.0%. Additionally, as it can be seen from the last rows of Tables 1 and 2, the residual errors of conductance and susceptance measurement at the level of 0.01% occur even at relatively low frequencies (10 Hz – 10 kHz). This is an indirect confirmation of the adequacy degree of the obtained simplified model of the auto-balancing bridge (14) on the basis of which correction algorithms have been synthesized.

Figures 5 and 6 show the results of measuring the admittance components to visualize the effectiveness of extending the frequency range of the auto–balancing bridge using correction algorithms.

In both Figures the dashed line shows the measurement results before correction, where the solid line – results after application of the proposed correction algorithms.

$$\begin{cases} \mathrm{P} - \dfrac{\mathrm{P}}{\mathrm{K}}(\mathrm{B}+\mathrm{C})(1+\mathrm{D}) - \dfrac{\mathrm{Q}}{\mathrm{K}}[1+\mathrm{G}(1+\mathrm{D})] = \mathrm{G} + \mathrm{B}\dfrac{\mathrm{D}}{\mathrm{K}} \\ \mathrm{Q} - \dfrac{\mathrm{Q}}{\mathrm{K}}(\mathrm{B}+\mathrm{C})(1+\mathrm{D}) + \dfrac{\mathrm{P}}{\mathrm{K}}[1+\mathrm{G}(1+\mathrm{D})] = \mathrm{B} - \mathrm{G}\dfrac{\mathrm{D}}{\mathrm{K}} \end{cases} \tag{26}$$

$$\begin{cases} \mathrm{G}\left[1+\mathrm{Q}\dfrac{(1+\mathrm{D})}{\mathrm{K}}\right] + \mathrm{B}\dfrac{[\mathrm{D}+\mathrm{P}(1+\mathrm{D})]}{\mathrm{K}} = \mathrm{P}\left[1-\mathrm{C}\dfrac{(1+\mathrm{D})}{\mathrm{K}}\right] - \dfrac{\mathrm{Q}}{\mathrm{K}} \\ -\mathrm{G}\dfrac{[\mathrm{D}+\mathrm{P}(1+\mathrm{D})]}{\mathrm{K}} + \mathrm{B}\left[1+\mathrm{Q}\dfrac{(1+\mathrm{D})}{\mathrm{K}}\right] = \mathrm{Q}\left[1-\mathrm{C}\dfrac{(1+\mathrm{D})}{\mathrm{K}}\right] + \dfrac{\mathrm{P}}{\mathrm{K}} \end{cases} \tag{27}$$

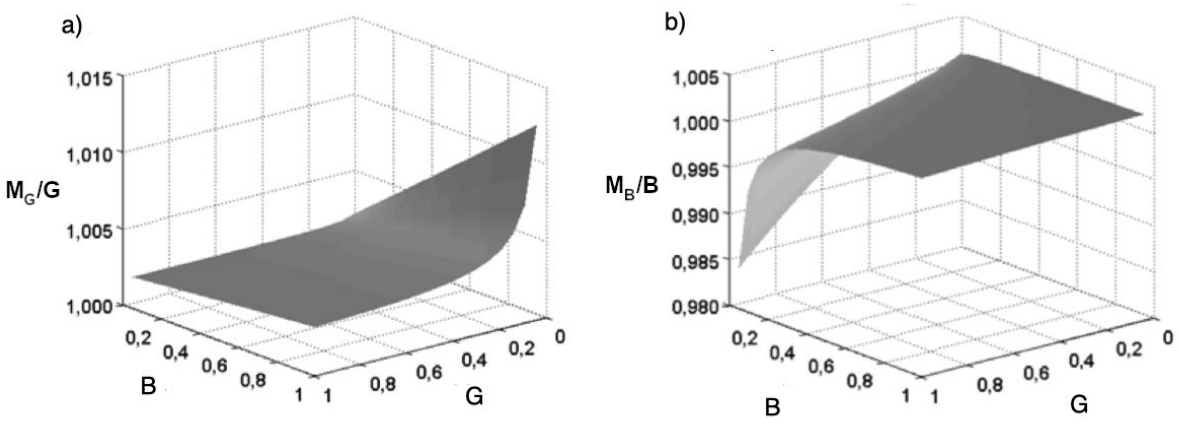

FIGURE 4. Estimate of the measurement accuracy of the relative value of conductance (a) and susceptance (b) on the phase plane.

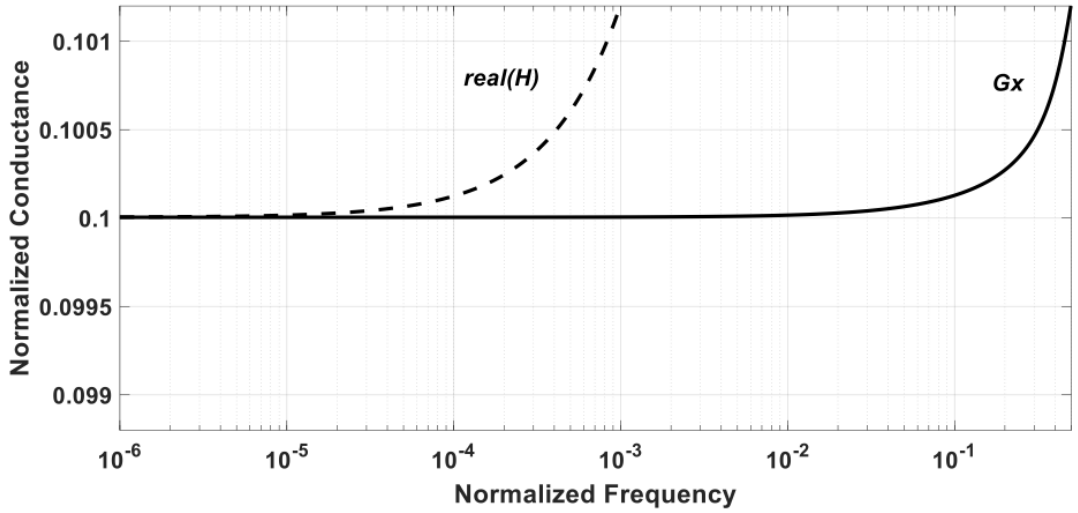

FIGURE 5. Measurement results: conductance of the tested object with admittance $Y_X = 10 + j100\,[\mu S]$.

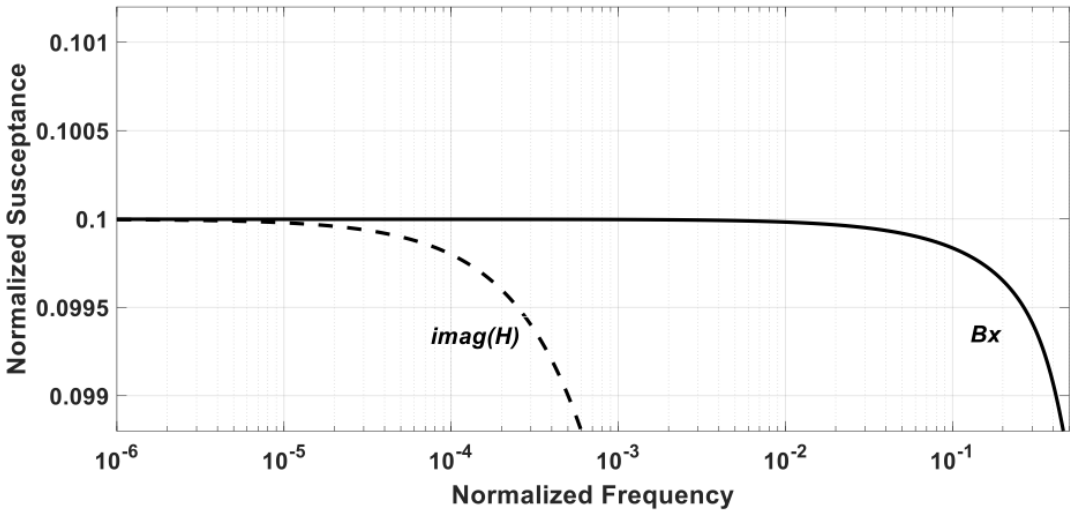

FIGURE 6. Measurement results: susceptance of the tested object with admittance $Y_X = 100 + j10\,[\mu S]$.

To maintain the generality of results and the ability to perform comparative analysis, the frequency responses of the auto-balancing bridge were given on a relative frequency f/f_T scale.

IV. DISCUSSION

Modelling results, performed by the authors of this work, show the effectiveness of correction algorithms in minimization of dynamic errors in auto-balancing bridge, as well as the ability to extend the frequency range of measurement. In both cases, the errors did not exceed **1**% for the frequency up to $f = 0.4\, f_T$ for the corrected results, while without the correction this limit was below the proposed $f = 0.001\, f_T$. Operating in absolute quantities, it is possible to state that the implementation of the algorithms (36) and 37 gives the possibility to extend the frequency range of the impedance meter from about 10 kHz to over 4 MHz if the auto–balancing bridge is built using operational amplifier with the unity gain frequency $f_T = 16\, MHz$.

The auto–balancing bridge operating frequency range can be extended with using operational amplifier with a greater importance of unity gain frequency, for example OPA837 ($f_T = 105\, MHz$) [36].

V. CONCLUSION

Impedance measurements are widely used in many fields of science and technology to study a variety of objects, including non-technical ones. Among the various impedance measurement techniques the auto–balancing bridge method is important, combining advantages such as measurement speed and relatively simple implementation, however the dynamic errors limit the operating frequency range.

The authors proposed and described in this work an innovative approach in minimizing of dynamic error based on the synthesis and use of correction algorithms. The algorithms presented in this work allow the correction of admittance measurements to be only based on ''raw'' results obtained with the use of an auto–balancing bridge. Missing values of parameters used in the correction algorithms can be calculated using the results obtained during calibration of the measuring channel using a reference resistor.

As shown in this work, developed correction algorithms allow to significantly extend (**400** times) the range of admittance measurement frequencies. These algorithms do not require changes in structure of the auto-balancing bridge, but only involve the computing power, which are already equipped with modern measuring devices. The scope includes a detailed description of the method of synthesis of algorithms aimed at reducing dynamic errors of only auto-balancing bridge section, which is the basic part of the impedance measurement system and testing their effectiveness. Hence, to focus exceptionally on auto-balancing bridge section errors, we intentionally assume that vector voltmeter (VVM) works perfectly.

The innovation of the proposed solution is based on the use of computational power in order to correct dynamic errors, and not to introduce the structural redundancy, as it is used in already known solutions. In order to implement such a solution in practice it is necessary to synthesize appropriate algorithms, which is the essence of the matter. The scope of the article includes the description of the structure of multi-frequency meter based on the auto-balancing bridge method, analysis and formalization of the mathematical model of auto-balancing bridge circuit, constituting the basis for the synthesis of correction algorithms.

The scope of the article also includes a description of the methodology for testing the effectiveness of the above algorithms. The results of the numerical simulation carried out on the PSpice model showed that the proposed solution extends the frequency range of admittance measurement 400 times, by omitting other sources of error.

The authors of this work decided to focus only on the operation of the auto-balancing bridge section. Analysis of operation of vector voltmeter and generator was not part of this work.

In the past – some of the authors of this work were involved in studies of similar applications but with different approach, so in work [37] the ABB dynamic error correction method was presented, where the range of feedback couplings for the application of I_Z power balancing flowing through the tested object, were applied. Unlike in the known approach: [13], the registers of sequence approximation were used for digital integration, which are also the output of the system. This affects the balancing process. This affects the balancing process. In terms of automation and automatic control, such impedance meters: [13], [38] are static systems, while the one presented in [37] is an astatic one. In order to shorten the balancing time, in paper [39] virtualizing the final balancing step was proposed. The hardware part of the impedance meter plays a minimal role in the balancing process (only at the final stage). It allows to improve the speed of components measurement about 10 times. A common feature of solutions [37], [39] is elimination of errors not only of the ABB section, but also of VVM. The cost of such solution are both time and hardware redundancy.

A. FURTHER RESEARCH PLANS

The following ideas might be interesting as potential future research topics:

- examination of the impact on the algorithms of correction of deviations from the nominal values of operational parameters amplifier such as: f_T, C_{IN}, R_{OUT}, occurring in the models of auto–balancing bridge and the proposed correction algorithms;
- development of the measurement procedure and calculation of the mentioned OpAmp parameters on the basis of data obtained at the calibration stage of the measurement path.

It would also be good to combine bioelectrical impedance spectroscopy with other measurement methods such as ECG or EEG [40]–[42]. Except measuring body structure, it would be also possible to detect stress or some serious conditions [10], [41]. Potential implementation of impedance in medicine is related with fact that it reflects also the change in blood pressure, and that the obtained results are very accurate [10].

Inter alia studies described here: [37] prove that implementation of auto–balancing bridge methods for this purpose gave very good results.

Implementation of auto-balancing bridge methods give positive results and they provide a very good impedance measurement accuracy. The authors of this work are planning to further explore this research area including incorporating other impedance measurement methods [39], [43].

REFERENCES

[1] J. R. Macdonald and E. Barsoukov, "Impedance spectroscopy: Theory, experiment, and applications," *History*, vol. 1, no. 8, pp. 1–13, 2005.
[2] V. F. Lvovich, *Impedance Spectroscopy: Applications to Electrochemical and Dielectric Phenomena*. Hoboken, NJ, USA: Wiley, 2012.
[3] S. Khalil, M. Mohktar, and F. Ibrahim, "The theory and fundamentals of bioimpedance analysis in clinical status monitoring and diagnosis of diseases," *Sensors*, vol. 14, no. 6, pp. 10895–10928, Jun. 2014.
[4] A. Nowakowski, T. Palko, and J. Wtorek, "Advances in electrical impedance methods in medical diagnostics," in *Bulletin of the Polish Academy of Sciences: Technical Sciences*. 2005, pp. 231–243.
[5] R. Zangróniz, A. Martínez-Rodrigo, J. Pastor, M. López, and A. Fernández-Caballero, "Electrodermal activity sensor for classification of Calm/Distress condition," *Sensors*, vol. 17, no. 10, p. 2324, Oct. 2017.
[6] J. Calvo-de la Rosa, J. Tejada, and A. Lousa, "Structural and impedance spectroscopy characterization of soft magnetic materials," *J. Magn. Magn. Mater.*, vol. 475, pp. 570–578, Apr. 2019.
[7] J. Hoja and G. Lentka, "A family of new generation miniaturized impedance analyzers for technical object diagnostics," *Metrol. Meas. Syst.*, vol. 20, no. 1, pp. 43–52, Mar. 2013.
[8] D. Xu, X. Cheng, S. Huang, and M. Jiang, "Identifying technology for structural damage based on the impedance analysis of piezoelectric sensor," *Construct. Building Mater.*, vol. 24, no. 12, pp. 2522–2527, Dec. 2010.
[9] F. Soulier, A. Lamlih, V. Kerzerho, and S. Bernard, "A multitone analysis for bioimpedance spectroscopy using minimal digital ressource," in *Proc. 12th Int. Conf. Sens. Technol. (ICST)*, Dec. 2018, pp. 315–318.
[10] I. Mohino-Herranz, R. Gil-Pita, M. Rosa-Zurera, and F. Seoane, "Activity recognition using wearable physiological measurements: Selection of features from a comprehensive literature study," *Sensors*, vol. 19, no. 24, p. 5524, Dec. 2019.
[11] P. J. Riu, J. Rosell, A. Lozano, and R. Pallà-Areny, "Multi-frequency static imaging in electrical impedance tomography: Part 1 instrumentation requirements," *Med. Biol. Eng. Comput.*, vol. 33, no. 6, pp. 784–792, Nov. 1995.
[12] T. Cannon and J. Choi, "Development of a segmental bioelectrical impedance spectroscopy device for body composition measurement," *Sensors*, vol. 19, no. 22, p. 4825, Nov. 2019.
[13] L. Callegaro, "On strategies for automatic bridge balancing," *IEEE Trans. Instrum. Meas.*, vol. 54, no. 2, pp. 529–532, Apr. 2005.
[14] L. Callegaro, V. D'Elia, J. Kucera, M. Ortolano, F. Pourdanesh, and B. Trinchera, "Self-compensating networks for Four-Terminal-Pair impedance definition in current comparator bridges," *IEEE Trans. Instrum. Meas.*, vol. 65, no. 5, pp. 1149–1155, May 2016.
[15] L. Callegaro, *Electrical Impedance: Principles, Measurement, and Applications*. Boca Raton, FL, USA: CRC Press, 2012.
[16] D. B. Kim, K.-T. Kim, M.-S. Kim, K. M. Yu, W.-S. Kim, and Y. G. Kim, "All-around dual source impedance bridge," in *Proc. Conf. Precis. Electromagn. Meas.*, Jul. 2012, pp. 592–593.
[17] J. Lan, Z. Zhang, Z. Li, Q. He, J. Zhao, and Z. Lu, "A digital compensation bridge for R–C comparisons," *Metrologia*, vol. 49, no. 3, p. 266, 2012.
[18] K. Okada and T. Sekino, "The impedance measurement handbook. a guide to measurement technology and techniques," App. Note, 2016.
[19] A. Bate, "Modern impedance measurement techniques," *Electron. World*, vol. 108, no. 1800, pp. 12–18, 2002.
[20] *AD 5933. 1 MSPS, 12 bit Impedance Converter, Network Analyzer. Preliminary Data Sheet*, Analog Devices, Norwood, MA, USA, 2020.
[21] *AD 5934, 250 KSPS, 12 Bit Impedance Converter Network Analyzer. Preliminary Data Sheet*, Analog Devices, Norwood, MA, USA, 2020.
[22] L. Matsiev, "Improving performance and versatility of systems based on single-frequency DFT detectors such as AD5933," *Electronics*, vol. 4, no. 1, pp. 1–34, Dec. 2014.
[23] B. Stadnyk and Y. Khoma, "Improving the accuracy of the single chip impedance analyzer for sensor applications," *Sensors Tranducers*, vol. 150, no. 3, p. 27, 2013.
[24] G. Li, M. Zhou, F. He, and L. Lin, "A novel algorithm combining oversampling and digital lock-in amplifier of high speed and precision," *Rev. Sci. Instrum.*, vol. 82, no. 9, Sep. 2011, Art. no. 095106.
[25] S. Sun, L. Xu, Z. Cao, H. Zhou, and W. Yang, "A high-speed electrical impedance measurement circuit based on information-filtering demodulation," *Meas. Sci. Technol.*, vol. 25, no. 7, Jul. 2014, Art. no. 075010.
[26] F. Soulier, A. Lamlih, V. Kerzérho, S. Bernard, and T. Rouyer, "Very low resource digital implementation of bioimpedance analysis," *Sensors*, vol. 19, no. 15, p. 3381, Aug. 2019.
[27] *Impedance Measurement Handbook. User's Guide*, 1st ed. HIOKI E.E. Corporation, Nagano, Japan, 2018.
[28] N. Li, H. Xu, W. Wang, Z. Zhou, G. Qiao, and D. D.-U. Li, "A high-speed bioelectrical impedance spectroscopy system based on the digital auto-balancing bridge method," *Meas. Sci. Technol.*, vol. 24, no. 6, Jun. 2013, Art. no. 065701.
[29] J. Prado, C. Margo, M. Kouider, and M. Nadi, "Auto balancing bridge method for bioimpedance measurement at low frequency," *Cell*, vol. 10, p. 3, Nov. 2005.
[30] N. Li, H. Xu, Z. Zhou, Z. Sun, X. Xu, and W. Wang, "Wide bandwidth cell impedance spectroscopy based on digital auto balancing bridge method," in *Proc. IEEE Biomed. Circuits Syst. Conf. (BioCAS)*, Nov. 2011, pp. 53–56.
[31] *Analog Devices, A Technical Tutorial on Digital Signal Synthesis*, Analog Devices, Norwood, MA, USA, 1999.
[32] *Low Power, 12.65 mW, 2.3 V to 5.5 V, Programmable Waveform Generator AD9833. DataSheet*, Analog Devices, Norwood, MA, USA, 2013.
[33] J. Dostal, *Operational amplifiers*. Amsterdam, The Netherlands: Elsevier, 2013.
[34] W. Jung, *Op Amp Applications Handbook*. Newnes, 2005.
[35] *AD845, Precision, 16 MHz CBFET Op Amp. DataSheet*, Analog Devices, Norwood, MA, USA, 2003.
[36] *OPAx837 Low-Power, Precision, 105-MHz, Voltage-Feedback Op Amp*, Texas Instruments, Dallas, TX, USA, 2003.
[37] T. Huynh, R. Jafari, and W.-Y. Chung, "An accurate bioimpedance measurement system for blood pressure monitoring," *Sensors*, vol. 18, no. 7, p. 2095, Jun. 2018.
[38] V. Khoma and M. Wrzuszczak, "Compensation admittance meter," *Przeglad Elektrotechniczny*, vol. 84, no. 5, pp. 33–36, 2008.
[39] D. Stepins, G. Asmanis, A. Asmanis, and L. Ribickis, "Measuring impedances of DC-biased inductors by using vector network analyzers," *Int. J. Electron. Telecommun.*, vol. 65, no. 3, pp. 375–380, 2019.
[40] R. Martinek, J. Brablik, J. Kolarik, M. Ladrova, J. Nedoma, R. Jaros, L. Soustek, R. Kahankova, M. Fajkus, L. Vojtisek, P. Hanzlikova, and P. Krupa, "A low-cost system for seismocardiography-based cardiac triggering: A practical solution for cardiovascular magnetic resonance imaging at 3 tesla," *IEEE Access*, vol. 7, pp. 118608–118629, 2019.
[41] R. Jaros, R. Martinek, and R. Kahankova, "Non-adaptive methods for fetal ECG signal processing: A review and appraisal," *Sensors*, vol. 18, no. 11, p. 3648, Oct. 2018.
[42] A. Kawala-Sterniuk, M. Podpora, M. Pelc, M. Blaszczyszyn, E. J. Gorzelanczyk, R. Martinek, and S. Ozana, "Comparison of smoothing filters in analysis of EEG data for the medical diagnostics purposes," *Sensors*, vol. 20, no. 3, p. 807, Feb. 2020.
[43] R. Sakai and S. Nakatake, "An impedance measurement of intravesical urine volume appropriate to seated posture," in *Proc. IEEE Asia–Pacific Conf. Circuits Syst. (APCCAS)*, Nov. 2019, pp. 385–388.

YURIY KHOMA was born in 1989. He received the M.Sc. degree in process measurement and sensor technology from the Ilmenau University of Technology, Germany, in 2001, and the Ph.D. degree in the field of measuring equipment and metrology, in 2014. He is currently employed as an Assistant Professor with the Institute of Computer Technology, Automatics and Metrology, Lviv Polytechnic National University. His scientific interests include artificial intelligence, bioinformatics, sensors, and electrical measurements.

VOLODYMYR KHOMA was born in 1959. He received the M.Sc. degree in automation and telemechanics, and the Ph.D. and Habilitation degrees in electrical and electronic engineering from the Lviv Polytechnic National University, Lviv, Ukraine, in 1981, 1990, and 2001, respectively.

He received the title of Professor in the field of control engineering in 2003. He is currently employed as a Professor with the Institute of Control Engineering, Opole University of Technology, Opole, Poland, and also with the Department of Information Security, Lviv Polytechnic National University. His scientific interests include principles and methods of using artificial intelligence in cybersecurity, cybersecurity of embedded systems and the IoT, methods and algorithms of digital measurement, and signal processing.

MICHAL PODPORA (Member, IEEE) was born in 1979. He received the B.Sc. and M.Sc. degrees in computer engineering and the Ph.D. degree in control engineering and robotics from the Opole University of Technology, Opole, Poland, in 2002, 2004, and 2012, respectively.

Since 2010, he has been the Research Department Manager and Project Manager of research projects for industry. He is currently employed as a Humanoid Robot Developer with the Research Department, Weegree, Opole, and as an Assistant Professor with the Institute of Computer Science, Opole University of Technology. His main research interests include artificial intelligence in robotics, machine vision, cognitive systems, robotic systems, smart infrastructure, embedded systems, the IoT, cybersecurity, and forensic science.

ALEKSANDRA KAWALA-STERNIUK (Member, IEEE) was born in Poland, in 1984. She received the M.Sc. degree in computer engineering from the Opole University of Technology, Opole, in 2007, and the Ph.D. degree in computing and mathematical sciences from the University of Greenwich in London, in 2013. In 2013, she started working as an Assistant Professor with the Opole University of Technology. In 2016, she was working with the University of Kentucky, Lexington, KY, USA, as a Postdoctoral Researcher. She has published nearly 100 papers. Her research interests include signal processing, biomedical data analysis, and digital filtering.

RADEK MARTINEK (Member, IEEE) was born in Czech Republic, in 1984. He received the master's degree in information and communication technology from the VSB-Technical University of Ostrava, in 2009.

Since 2012, he was working as a Research Fellow with the VSB-Technical University of Ostrava. In 2014, he successfully defended his dissertation thesis "Use of Complex Adaptive Methods of Signal Processing for Refining the Diagnostic Quality of the Abdominal Fetal Electrocardiogram." He became an Associate Professor of technical cybernetics in 2017, after defending the habilitation thesis "Design and Optimization of Adaptive Systems for Applications of Technical Cybernetics and Biomedical Engineering Based on Virtual Instrumentation." He has been an Associate Professor with the VSB-Technical University of Ostrava, since 2017. His current research interests include digital signal processing (linear and adaptive filtering, soft computing—artificial intelligence and adaptive fuzzy systems, non-adaptive methods, biological signal processing, digital processing of speech signals), wireless communications (software-defined radio), and power quality improvement. He has more than 200 journals and conference articles in his research areas.

STEPAN OZANA was born in Bilovec, Czech Republic, in May 1977. He studied electrical engineering at the VSB Technical University of Ostrava, and received the M.Sc. degree in control and measurement engineering, in 2000, and the Ph.D. degree in technical cybernetics, in 2004.

In 2015, he was habilitated in technical cybernetics. Since then, he has been working as an Associate Professor with the Department of Cybernetics and Biomedical Engineering, Faculty of Electrical Engineering and Computer Science, VSB-Technical University of Ostrava. He currently gives lectures on cybernetics and control systems. His main areas of interest and expertise are modeling and simulation of dynamic systems, control theory, automation, design, implementation, and deployment of control algorithms using softPLC systems.